Available online at www.sciencedirect.com

SciVerse ScienceDirect

Ceramics International 38 (2012) 6531–6540

CERAMICS INTERNATIONAL

www.elsevier.com/locate/ceramint

Preparation of photocatalytic TiO_2 coatings by gel-dipping with polysaccharides

Isabel Santacruz*, Aurelio Cabeza, Paul Ibeh, Enrique R. Losilla, Ángeles G. De la Torre, Miguel A.G. Aranda

Departamento de Química Inorgánica, Cristalografía y Mineralogía, Universidad de Málaga, 29071-Málaga, Spain

Received 20 March 2012; received in revised form 30 April 2012; accepted 10 May 2012
Available online 17 May 2012

Abstract

Commercial tiles are being produced in vast quantities. The main properties of tiles are well established but there is an increasing interest in producing ceramics with tailored-properties and advanced functionalities. One way of adding value to commercial tiles is to deposit a photocatalytic coating to obtain 'smart' tiles for environmental reasons, e.g. for the (photo) degradation of organic pollutants in air or in a liquid. Here, we show the manufacture of 'smart' tiles by formation of TiO_2 coatings onto commercial tiles by a colloidal processing route based on the immersion of the substrate into a homogeneous aqueous ceramic suspension and its consolidation by agar thermogelation. The effect of the processing parameters (withdrawal rate, solid loading and gelling agent content) and the grain size on the photocatalytic activity of the final coated tiles is reported and discussed. Final coatings properties depend on the viscosity of the suspension, particle size, withdrawal rate, solid loading and gelling agent content, and hence, this dependence affects the photocatalytic activity of the coatings.

Keywords: A. Films; A. Suspensions; D. TiO_2; E. Functional applications

1. Introduction

Titania ceramics, TiO_2, are widely used as sensors and solar energy cells; titania is a promising photocatalyst [1], so it is receiving a lot of attention in the field of environmental protection. Titania occurs naturally as rutile, anatase and brookite phases. The rutile and anatase phases have been deeply studied and have significant technological uses related to their optical properties. Rutile surface is used as a prototypical model for basic studies of oxide surfaces. Anatase is the most photoactive phase of TiO_2, but only absorbs ultraviolet light with wavelengths shorter than 380 nm. The size of the titania particle/grain is an important factor to improve photocatalytic activity [2]. Nanocrystalline materials display unusual properties, including high photovoltaic, electro-optical, and also high hardness and strength, and low sintering temperatures, offering the ability to save energy [3–5]. Other parameters evolved in the photocatalytic activity are the porosity, surface area, sintering temperature, or if TiO_2 is used as powder, as a tape/coating, as a bulk, or in cementitious systems [6–8].

There are many simple organic substances which are degraded in presence of TiO_2 and UV radiation, such as methyl orange [9,10], rhodamine B [2], phenol and acetaldehyde [11], benzotriazole [12], sodium dodecylbenzene sulphonate surfactant [13], etc., and they are being used as tests for characterising the photocatalytic activities.

As a photocatalyst, TiO_2 is mostly used in the form of thin films [10,11,14] or powder [15–17], the latter providing the best results. However, the use of particulate TiO_2 shows environmental and technological inconveniences related to recycling and management. Thus, obtaining photocatalysts with designed physicochemical properties is a key point in the process. There are a wide number of thin-film deposition methods to form layers such as evaporative processes, glow-discharge technologies,

*Corresponding author. Tel.: +34 952 13 1992; fax: +34 952 13 1870.
E-mail address: isantacruz@uma.es (I. Santacruz).

0272-8842/$36.00
http://dx.doi.org/10.1016/j.ceramint.2012.05.034

gas-phase chemical processes or liquid-phase chemical formation [18].

A well dispersed suspension is required when evaporative processes are evolved. In colloidal processing, the dispersion of ceramic powders in either an aqueous or a non-aqueous medium has received considerable attention [19,20]. To achieve adequate distance between particles in ceramic suspensions generally requires the use of surfactants that modify the particle surface. However, it is well known that stable slurries with a high solid loading and a low viscosity use to be required for many colloidal processes, and this is difficult to achieve with particles in the sub 100 nm range [21,22]. Colloidally stable nanopowder suspensions are known to display a markedly lower volume loading at the same viscosity compared to suspensions with larger particle sizes [23]. Organic solvents are commonly used for coatings processing; however, for economical and environmental reasons, the current tendency is the use of aqueous systems. The simplest method to produce coatings onto a variety of substrates is the dipping method, which is extensively used in several technologies like sol–gel processing. However, most ceramic suspensions, especially those prepared in aqueous systems, do not properly wet the substrates and no coatings can be obtained by simply dipping. The wetting and adherence can be improved by using a gelling agent. The use of biopolymers that gelate on cooling has been successfully applied in the manufacture of near-net shaped bodies [24] in aqueous media. The forming mechanism involves: (i) preparation of an aqueous ceramic suspension and the addition of a small amount (≤ 1 wt%) of a suitable polysaccharide (e.g. agar, agarose, carrageenan) at temperatures above its glass transition temperature ($T_g \sim 40$ °C), (ii) filling of a mould cavity (by pouring or injection) and (iii) cooling of the mould below the T_g to allow consolidation by thermogelation [25]. Some attempts [26] have been described to extend the applications of polysaccharides gelation to the production of laminates and coatings by simply dipping the substrate in a suspension containing the gelling agent.

This work deals with the manufacture of tiles with tailored properties by the preparation of TiO_2 coatings onto commercial tiles by a colloidal processing route based on the immersion of the substrate (tile) into an aqueous ceramic suspension and its consolidation by agar thermogelation after withdrawal. The effect of the processing parameters (withdrawal rate, solid loading, gelling agent content and grain size) on the photocatalytic activity of the final coated tiles is reported and discussed.

2. Experimental procedure

Two sources of titania have been used: (i) commercial TiO_2–anatase powder (Merck, 808, Germany) with a particle size of $\sim$350 nm; and (ii) a commercial aqueous nanosuspension provided by Degussa (VP Disp W740X, Evonik Degussa Corporation, Germany) with $\sim$20 nm TiO_2 particles. The Rietveld quantitative phase analysis of the dried nanopowder obtained from that suspension gave 86.2(2)% anatase and 13.8(4) wt% rutile. Laboratory X-ray powder diffraction (LXRPD) patterns were collected on a PANalytical X'Pert Pro MPD automated diffractometer equipped with a Ge(111) primary monochromator (strictly monochromatic CuKα_1 radiation) and an X'Celerator detector (PANalytical B.V., Almelo, The Netherlands). The studied 2θ range was 10°–100° with a 0.017° step size. The solid loading was determined to be 40 wt% after drying the suspension in an oven at 65 °C overnight and studied through thermogravimetric analyses, TGA (Netzsch, STAY09, Germany) up to 1000 °C. The organic content of the suspension was 2.6 wt%. The pH of the as-received nanosuspension was 7.0.

On one hand, 80 mL submicronsized aqueous suspensions were prepared and optimised at a solid loading of 75 wt% (43.5 vol%, using 3.89 g cm^{-3} for anatase [27] theoretical density). An ammonium salt of polyacrylic acid, PAA, (Duramax D3005, Rohm & Haas, Pennsylvania, USA) with an average molecular weight of $\sim$2400 Da and a 35 wt% active matter was used as dispersant. The added deflocculant amount, 0–0.30 wt%, is always provided in terms of the percentage of active matter in the dispersant on dry solid basis. The suspensions were mechanical stirred with helices and then attrition milled with alumina balls for up to 1.5 h. Note that the milling was performed in 15 min steps, with the suspension being at room temperature for 10 min between each milling in order to avoid excessive heating of the suspension. The effect of the pH on the 75 wt% deflocculated suspensions was also studied (4.5–10.0). Once all the parameters were optimised, submicron suspensions with different solid loadings, 20, 40 and 65 wt% (6.0, 14.6, 32.3 vol%, respectively), were prepared.

On the other hand, the effect of pH (5.5–10.0) and PAA content (0–3.0 wt%) on the as-received nanosuspension was studied. Nanosuspensions with solid loadings of 40 wt% (14.5 vol%) and 20 wt% (6.0 vol%) were studied. Theoretical density values of 3.89 and 4.25 g cm^{-3} were used for anatase [27] and rutile [28], respectively.

The rheological behaviour of the suspensions was studied using a rotational viscometer (Model VT550, Thermo Haake, Karlsruhe, Germany) with a coaxial cylinder sensor, MV DIN, equipped with a solvent trap to reduce evaporation. Suspensions flow curves were obtained through controlled rate (CR) measurements at 25 °C using a three-stage measuring programme with a linear increase in the shear rate from 10 to 400 s^{-1} in 200 s, a plateau at 400 s^{-1} for 60 s, and a further decrease to 10 s^{-1} in 200 s. The evolution of the viscosity of the suspensions with temperature (during heating, 1.5 °C/min) and suspensions with agar (during cooling, 0.5 °C/min) was studied; a probe of temperature, which enables the continuous recording of viscosity data on heating or on cooling was used. All these tests were made at a constant shear rate of 50 s^{-1}. Before starting any rheological measurement the suspensions were presheared for 30 s at 50 s^{-1}.

As gelling agent, agar powder (Grand Agar, Hispanagar, Burgos, Spain) was used. A concentrated agar solution (6.0 wt%) was prepared under overpressure conditions using a pressure cooker [29] that allows to reach a temperature of ~110 °C. This agar solution was maintained at 55 °C and added to the slips which were also heated at 55 °C. The amount of added solution was that required to incorporate 0.5 and 1.0 wt% of agar powder with regard to the total water content. The concentration of gelling agent is expressed as a function of the total water content because it forms a 3D-structure during gelling by H-bonds between OH groups and water molecules.

As substrate, commercial ceramic tiles (K, Keramex S.A., Castellon, Spain) fabricated by dust pressing for internal wall finishes with original dimensions of 20 cm × 20 cm were used. Dipping experiments were performed by introducing commercial tiles (24 mm × 40 mm) into a well dispersed TiO_2 suspension (submicron or nanosuspension) which contains agar at 55 °C, and further withdrawal at constant rates of 5 or 15 mm s^{-1}. Green coated substrates were left at room temperature for 48 h to dry. The coating obtained outside the tile glaze was removed. The weight of the dry green deposits onto the tile glaze was measured by gravimetry. Finally, gel-cast coated tiles were sintered at 1000 °C for 1 h. A debinding cycle was not performed because commercial tiles were previously thermally treated in the factory (> 500 °C), and the added biopolymer content was very low.

Sintered coatings were characterised by LXRPD. Microstructures of the transversal section of the sintered samples were observed by scanning electron microscopy, SEM (JEOL-JSM-840, Tokyo, Japan). The photocatalytic activity of the coated tiles was studied through the degradation of a 10 mg/L methyl orange solution (MO) prepared at pH 2.0 (with HCl), as the best photocatalytic efficiency was described under those acidic conditions [9]. These experiments were conducted in a home-made photochemical reactor with mechanical stirring during the illumination to ensure a thorough mixing. A low-pressure mercury lamp (125 W) emitting at 365 nm was used in the photoreactor. The distance between the lamp and the sample was 20 cm. Selected sintered coated-samples (24 mm × 40 mm) were held in 100 mL of methyl orange solution. The degradation of the dye was studied after 0.5, 1.0, 2.0, 3.0, 4.0 and 4.5 h irradiation. The absorbance of the irradiated solutions was measured in a UV–vis spectrophotometer (UV-1800, Shimadzu, Kyoto, Japan) and the maximum MO absorbance resulted at 550 nm.

AFM (atomic force microscopy) experiments were conducted on selected coatings (top side) with a diMultiMode^{TM}V Nanoscope V AFM instrument (Digital Instruments-Veeco, Woodbury, NY, USA). Images were acquired in tapping mode in air with a sharp silicon probe (TESP, Veeco, Woodbury, NY, USA). The scanning data were processed and analysed with a NanoScope Analysis 1.40 software, Version R1Sr2.77483 (Bruker, Madison, WI, USA).

3. Results and discussion

The preparation of submicron TiO_2 suspensions was reported elsewhere [30]; however, the use of a different deflocculant and different milling conditions requires the optimisation of the suspension. Fig. 1a shows the flow curves of a 75 wt% submicron suspension with 0.2 wt% PAA at pH 5.5 and 25 °C after different milling times (0–1.5 h). All

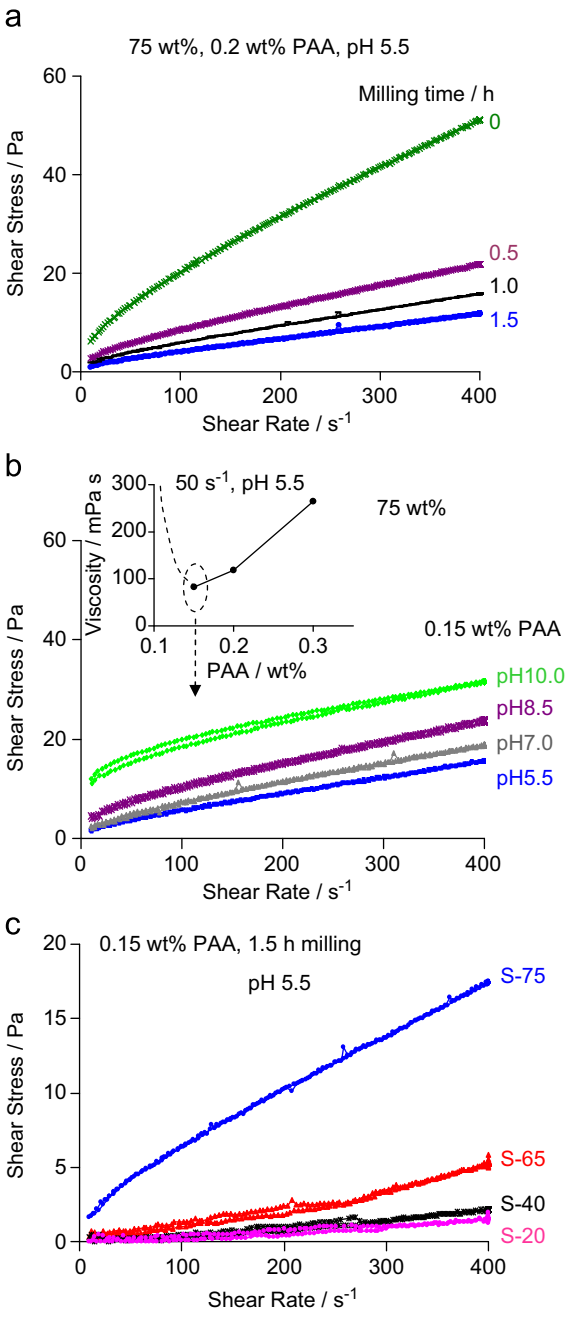

Fig. 1. Flow curves of 75 wt% submicron suspensions with 0.2 wt% PAA and different milling times (pH 5.5) (a); 75 wt% submicron suspension, 0.15 wt% PAA milled for 1.5 h, at different pH values (b); 75 wt% submicron suspension with 0.15 wt% PAA milled for 1.5 h, at different solid loadings (pH 5.5) (c). The inset of Fig. 1b corresponds to the deflocculation curve of the submicron suspension (75 wt%, milled for 1.5 h) at 50 s^{-1}.

the suspensions show a shear thinning behaviour without thixotropy. The viscosity decreases with the milling time by breaking agglomerates. Longer milling times were not studied in order to avoid contamination from the balls. Once the milling time was selected (1.5 h), the deflocculant content was optimised. The inset of Fig. 1b shows the deflocculation curve (50 s^{-1}) of the submicron suspension, where the minimum viscosity value was achieved after the addition of 0.15 wt% PAA (milled for 1.5 h). Isoelectric point (IEP) values are ~4.2 and ~3.2 for commercial submicron powder and nanopowder from commercial nanosuspension, respectively. The lower IEP of the nanoparticles is related with the adsorption of the organics present in the nanosuspension. In the case of submicron powder, the addition of PAA shifts down its IEP to ~2.0 [31]. The effect of the pH on the deflocculated submicron suspension (0.15 wt%) at 25 °C is shown in Fig. 1b. The pH of the as-prepared submicron suspensions was 5.5. Submicron suspensions showed low viscosity values at pH between 5.5 and 8.5, (70, 89 and 145 mPa s at 50 s^{-1}, for pH values of 5.5, 7.0 and 8.5, respectively). However, at pH 10.0 and 4.5 the viscosity increased (305 and > 350 mPa s at 50 s^{-1}, respectively). Hence, the suspensions can be prepared easily at pH values between 5.5 and 8.5. Thus, further submicron suspensions were prepared at pH 5.5.

Once the concentrated (75 wt%) submicron suspension was optimised, submicron suspensions were prepared at different solid loadings, 65, 40 and 20 wt% (pH 5.5). Fig. 1c shows the flow curves (25 °C) of submicron suspensions at different solid loadings, 75, 65, 40 and 20 wt%, called hereafter as S-75, S-65, S-40 and S-20. Coatings prepared from 75 wt% submicron suspensions were dense and thick hence, they showed lack of adherence. Because of that, 75 wt% suspensions were not further studied.

The effect of pH (5.5–10.0) and PAA content (0–3.0 wt%) on the as-received nanosuspension (40 wt%) was also studied. The nanosuspension resulted to be homogeneous from pH 5.5 to 9.0; however the viscosity increased at pH 10.0, as submicron suspensions did. The viscosity also increased by the addition of PAA (e.g. from 14 to 32, 231 and 262 mPa s, at 50 s^{-1}, after the addition of 1, 2 and 3 wt% PAA, respectively). From these results, the nanosuspensions (40 and 20 wt%, called hereafter as N-40 and N-20, respectively) were used at pH 7.0 for further studies without any addition of PAA. Nanosuspensions (N-40 and N-20) were adapted to the shaping method by the addition of agar solution.

Since suspensions have to be heated at 55 °C before the polysaccharide addition, the effect of the temperature on the suspensions needed to be studied. Fig. 2 shows the variation of viscosity during heating of 65 wt% submicron suspension and 40 wt% nanosuspension at 50 s^{-1}. The viscosity slightly decreases at the beginning of heating and then maintains nearly constant up to 70 and 62 °C for submicron and nanosuspensions, respectively. No destabilisation was observed at 55 °C, therefore these suspensions and more diluted ones can be used successfully for our purposes at that temperature. 40 wt% nanosuspension showed lower viscosity values (before destabilisation) than 65 wt% submicron suspension due to its lower solids content.

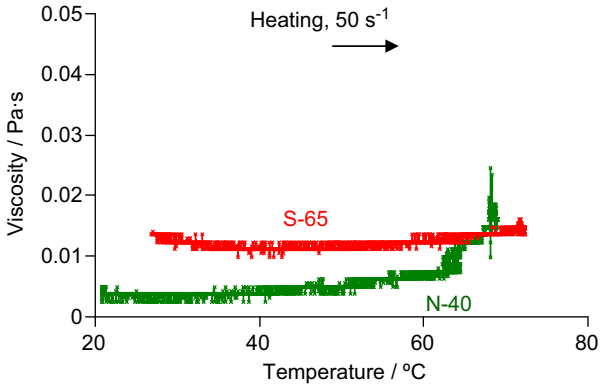

Fig. 2. Evolution of viscosity with temperature (on heating) for submicron suspensions (65 wt%) and nanosuspensions (40 wt%).

Fig. 3 shows the flow curves, measured at 55 °C, of S-65, S-40, S-20, N-40 and N-20 suspensions with 0.5 and 1.0 wt% agar (Figs. 3a and b, respectively). All the suspensions show a shear thinning behaviour without thixotropy. It is also observed that viscosity is mainly controlled by the concentration of agar, while the solids loading have a smaller effect. Thus, in the sol state, agar contributes to viscosity as a thickener. For the same solid loading, e.g. 40 wt%, the nanosuspension shows higher viscosity values than the corresponding submicron suspension and, in addition, this difference in viscosity is more remarkable for higher agar content. This is related to the lower primary particle size [23] and also to some interaction between the biopolymer and the nanoparticles [31].

On cooling, the viscosity tends to slightly increase following a linear evolution, and a sharp increase takes place at the gelling temperature. Fig. 4 shows the evolution of viscosity on cooling (shear rate: 50 s^{-1}) for the same suspensions showed in Fig. 3. Higher shear rate values would partially destroy the gels that are being formed. The T_g value increases with the content of agar in agreement with a previous work [32].

Dipping tests were performed using suspensions heated at 55 °C to prevent the additive gelation. The withdrawal rates were maintained constant at 5 and 15 mm s^{-1}. Suspensions without agar slipped from the ceramic substrate on withdrawal and no deposits could be obtained. Hence, agar is needed to guarantee adherence of the deposit to the substrate. After withdrawal from the hot suspension, the as-formed deposits gel at room temperature (20 °C) leading to homogeneous wet films. Fig. 5 plots the mass per unit area of the dry deposits obtained by dipping the tile into differently prepared suspensions. The deposited mass increases with the withdrawal rate, the agar content and the solids loading, and decreases by increasing the primary particle size; thus the mass increases by increasing the suspension viscosity.

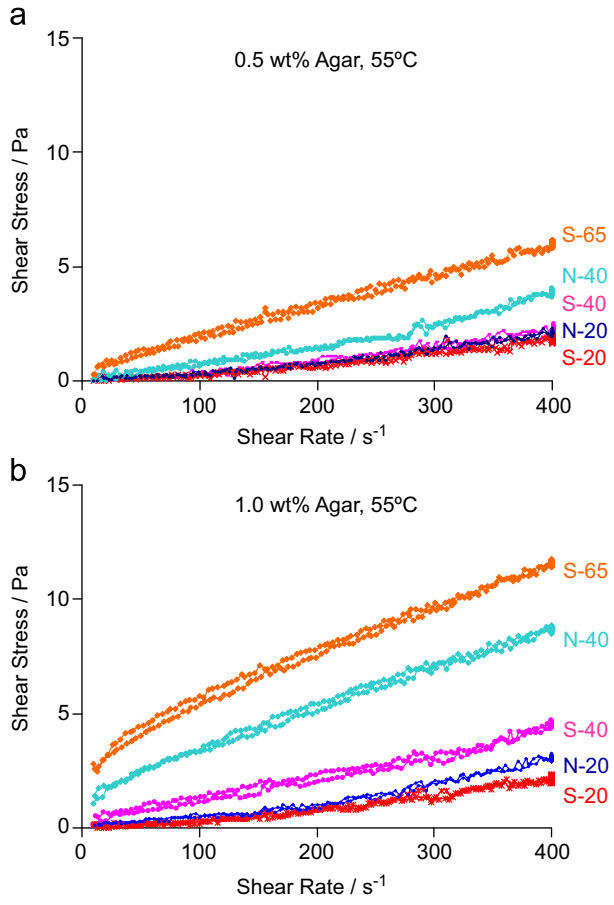

Fig. 3. Flow curves of submicron and nano-suspensions at different solid loadings with: 0.5 wt% (a) and 1.0 wt% (b) agar.

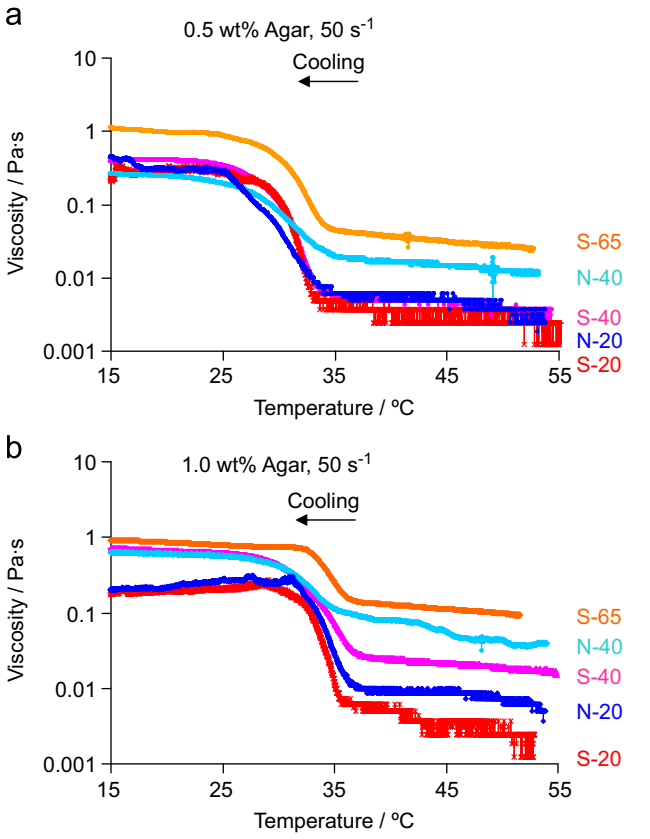

Fig. 4. Evolution of viscosity with temperature (on cooling) for submicron and nano-suspensions at different solid loadings with: 0.5 wt% (a) and 1.0 wt% (b) agar.

The most critical parameter that controls the stiffness of the gelled deposit in this study is the volume fraction of particles. If the formed coating is too thick, the cohesion of the deposit will exceed the adherence with the substrate and the resulting stiff and rigid gel will release on drying. This occurs in the case of the most concentrated suspensions, ≥ 65 wt% solids, with both 0.5 and 1.0 wt% agar, where the mass/area values are ≥ 150 g/m^2. Concentrated submicron suspensions (≥ 65 wt%) were not further studied due to delamination of the corresponding TiO_2 coatings after drying. Hence, the study was focused on 20 and 40 wt% suspensions where no delamination was observed. It is also important to consider the concentration of particles to achieve the desired consistency. The lowest concentration used in this work, 20 wt%, was good enough to produce thin homogeneous films. Furthermore, there are other parameters (withdrawal rate and agar content) which also have influence on the properties of the final coatings. Since the viscosity of a suspension increases by increasing the agar content for a fixed solid content (Figs. 3a and b), it is expected that suspensions with 1.0 wt% agar will produce thicker coatings than the corresponding suspensions with 0.5 wt% agar, according to $e_l = c_1(\eta v/\rho g)^{1/2}$where e_1 corresponds to the coating thickness, c_1 is a constant, η stands for the viscosity of the suspension, v for the withdrawal rate, ρ corresponds to the density of the suspension, and g is the gravitational acceleration.

Suspensions with 1.0 wt% agar will produce more porous coatings than those with lower agar content due to the slightly higher organic content which will be burnt out during sintering. To study the influence of different processing parameters onto the properties of the coatings, those marked with a cycle in Fig. 5 were deeply characterised.

The thickness of the sintered coatings was estimated by SEM observation at different magnifications (not shown), however this leads to some uncertainty so we give average values. Note that the shown coatings (Figs. 6b–e and 7) correspond to the area included between the discontinuous lines, and the material on the right side corresponds to the commercial tile. The reported thicknesses are approximate values because some coatings are not fully straight.

Fig. 6a shows the transversal section of a commercial tile observed by SEM at low magnification. The left part of the tile corresponds to the tile glaze which will be further coated. Fig. 6b and c show SEM micrographs of the fracture transversal sections of the sintered coatings obtained from S-40 suspensions with 1.0 wt% agar under withdrawal rates of 5 and 15 mm s^{-1}, respectively. Hereafter, these samples will be labelled as S-40-1.0-5 and S-40-1.0-15, respectively.

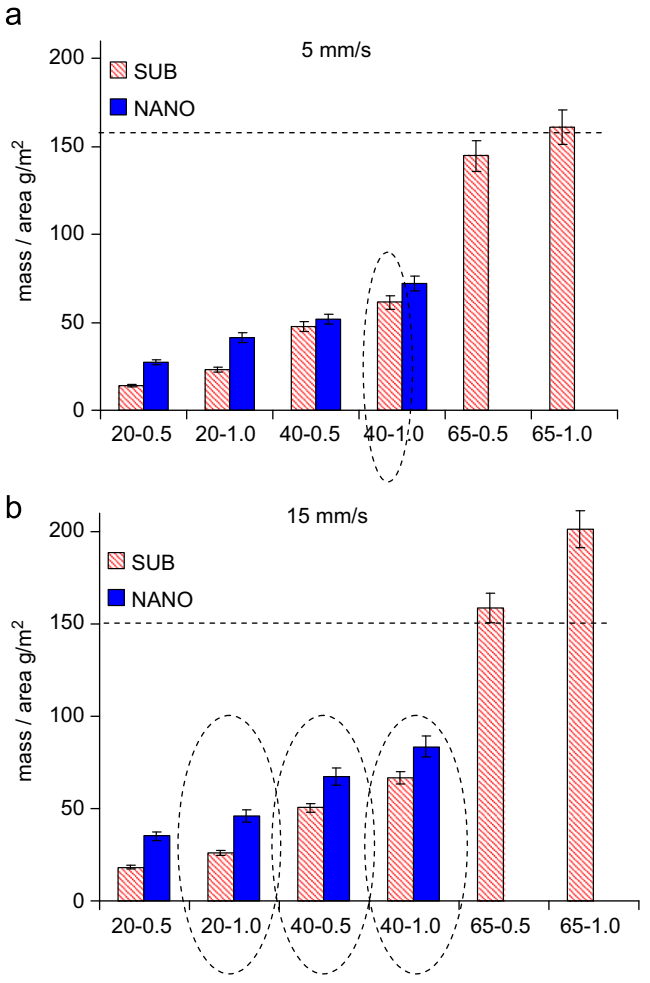

Fig. 5. Evolution of weight per unit area of green deposits obtained by gel-dipping from selected suspensions. Withdrawal rate: 5 mm s^{-1} (a) and 15 mm s^{-1} (b).

A thickness of ~5 μm was obtained for S-40-1.0-5; this value increased up to ~20 μm for coatings obtained from the same suspension when the withdrawal rate increased to 15 mm s^{-1} (S-40-1.0-15). Coatings prepared from 40 wt% suspension with 0.5 wt% agar and a withdrawal rate of 15 mm s^{-1} (S-40-0.5-15), Fig. 6d, showed an intermediate thickness (~15 μm). The effect of solid loading onto the thickness can be observed by comparing S-20-1.0-15 (Fig. 6e) and S-40-1.0-15 (Fig. 6c) coatings. The former shows a much thinner thickness (~3 μm), which corresponds approximately to the size of just one titania sintered grain.

Fig. 7 shows the effect of agar content and solid loading on nanostructured coatings; when a low agar content is added (N-40-0.5-15), Fig. 7a, the coating shows lower thickness (~7 μm) than the corresponding coating (~30 μm) with higher agar content (N-40-1.0-15), Fig. 7b. When the solid loading is reduced to 20 wt% (N-20-1.0-15), Fig. 7c, the coating is thinner (~2 μm) than that from the corresponding coating prepared with higher solid loading. Delamination was not observed in any sintered coating. Hence, well-adhered TiO_2 coatings with thicknesses between ~2 and ~30 μm can be prepared by this methodology with no delamination. The average grain size of coatings prepared from S-40 and S-20 suspensions after sintering at 1000 °C is ~1 μm and ~3 μm, respectively. Coatings obtained from nanosuspensions show grain sizes lower than 0.5 μm. The only phase detected by LXRD in all sintered coatings was rutile.

Although the obtained mass/area values for green nanocoatings are larger than those for submicron-coatings, nanostructured sintered coatings are thinner than microstructured coatings (Figs. 6 and 7, respectively). This is related to the higher densification of nanostructured coatings during sintering.

From these results, it can be concluded that the thickness increases by increasing withdrawal rate, solid loading and agar content, being the former the most important parameter, followed by the solid loading.

Fig. 8 gives a preliminary study of the photocatalytic activities of coated tiles during the degradation of a MO solution under UV-A radiation. These results are compared with an irradiated MO solution under the same conditions without TiO_2 (blank). Since all the samples contain the same phase (rutile), the observed differences in the dye photodegradation are mainly related with the physical properties of the coatings.

The decomposition rate model of this pollutant was evaluated by the equation $K=\ln[C_0/C_t]/t$ [33], where C_t stands for the concentration of reactant, C_0 corresponds to initial concentration of reactant, t is reaction time and K is pseudofirst-order rate constant. Table 1 shows the pseudofirst order rate constant, K, and the correlation factor value (R^2) for selected samples. Table 1 also shows the MO degradation after 2 and 3 h of irradiation.

The degradation efficiency of the specimen increases by decreasing the grain size, and by increasing the withdrawal rate, agar content and solid loading (Fig. 8). The tendency is very clear after 2 h of irradiation. MO solutions in presence of nanostructured coatings show higher degradation conversions than the corresponding microstructured coatings; e.g. degradation conversions in presence of S-40-1.0-5 and N-40-1.0-5 are 71 and 91%, respectively, and for S-40-0.5-15 and N-40-0.5-15 are 52 and 86%, respectively, after 2 h of irradiation. The effect of the agar content can be studied by comparing S-40-1.0-15 and S-40-0.5-15 coatings, where the former shows a higher MO degradation conversion (e.g. 71 and 52%, respectively, after 2 h of irradiation). This is related to a more porous coating (open porosity) for S-40-1.0-15 in combination with a thicker coating (due to the higher viscosity). These factors increase the contact area between the coating and the MO solution, and hence improve the photocatalytic activity. The influence of the withdrawal rate on the photocatalytic degradation of the MO solution is also given in Fig. 8. By increasing the withdrawal rate, the obtained coatings are thicker (see Figs. 6b and c) and, in combination with the open-porous coatings, a higher efficiency for MO degradation is achieved again.

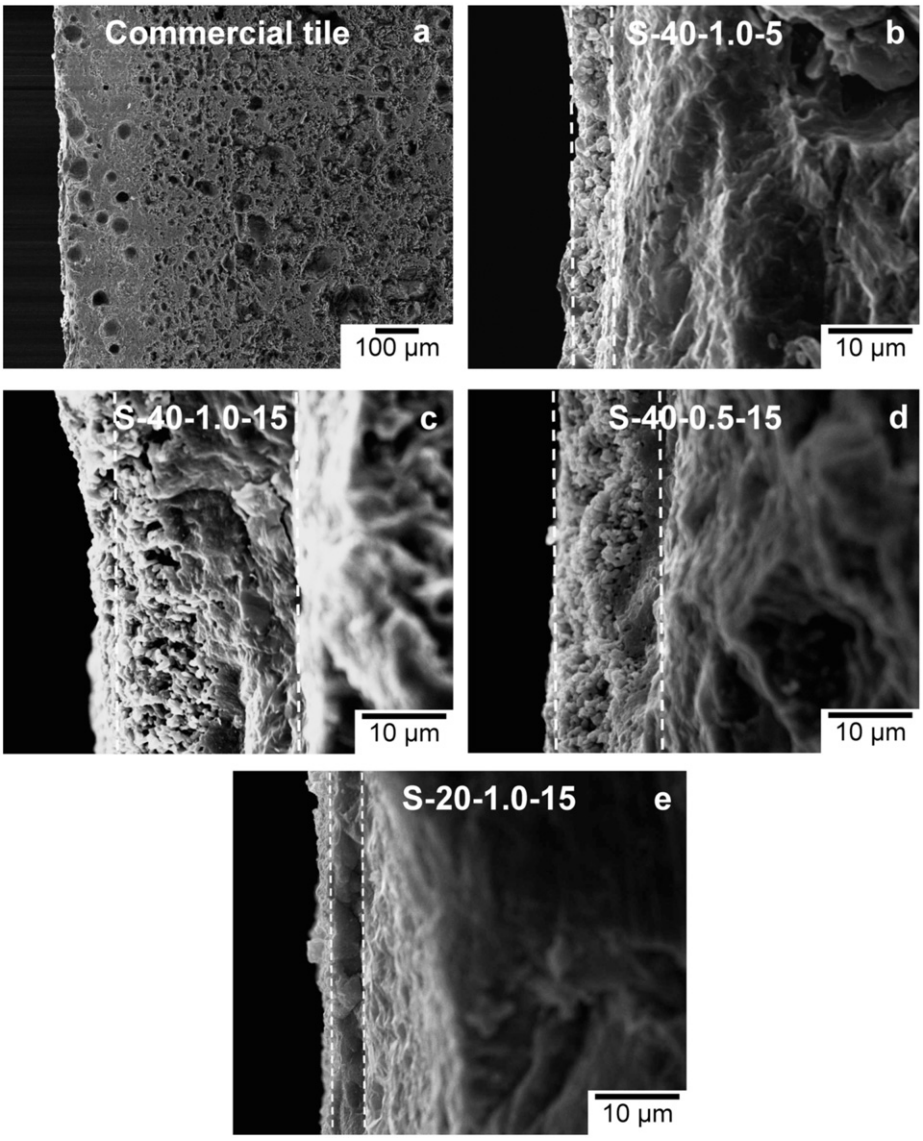

Fig. 6. Cross-sectional fracture surface microstructures (SEM) for: commercial tile (a), S-40-1.0-5 (b), S-40-1.0-15 (c), S-40-0.5-15 (d), and S-20-1.0-15 (e).

In the case of nanostructured coatings, these three parameters have lower effect onto the efficiency of the MO degradation, where N-40-0.5-15 and N-40-1.0-15 show a similar tendency at any irradiation time. MO degradation in presence of N-20-1.0-15 follows the same tendency after ≥ 2 h of irradiation. However, after 0.5 and 1 h of irradiation, N-20-1.0-15 shows only slightly higher efficiency than S-20-1.0-15. Heterogeneous photocatalysis is produced by the adsorption of organics onto the catalyst. Since it is a surface phenomenon, a good photocatalyst is expected to show high specific area and porosity values. Fig. 9 compares the topographic images (25 μm × 25 μm section) of S-40-1.0-5 and N-40-1.0-15 coatings (top side) obtained by AFM, Fig. 9a and b, respectively. The insets show smaller sections (5 μm × 5 μm) of the corresponding coatings. S-40-1.0-5 and N-40-1.0-15 coatings have been selected for comparison due to their different efficiency in MO degradation (see Fig. 8). The average roughness and ironed surface values (25 μm × 25 μm section) for S-40-1.0-5 are 319 nm and 730 μm^2, respectively. The corresponding values for N-40-1.0-15 are 287 nm and 673 μm^2, respectively, where some mesoporosity was observed. Although the microstructured coating shows higher values of roughness and ironed surface, its efficiency during MO degradation was lower. Hence, the better efficiency should be related with the nanostructure. It is known that the diffusion of electron/hole pairs through TiO_2 surface is quicker for nanostructured materials. Thus, the recombination of electron/hole pairs is less probable because it is quickly evolved in oxidation–reduction reactions [34]. Because of this, nanostructured materials are catalytically more efficient than microstructured ones.

According to the results, our obtained microstructured and nanostructured rutile-coatings are very promising since they show higher efficiency than those films reported in the literature, even when many of them show anatase as

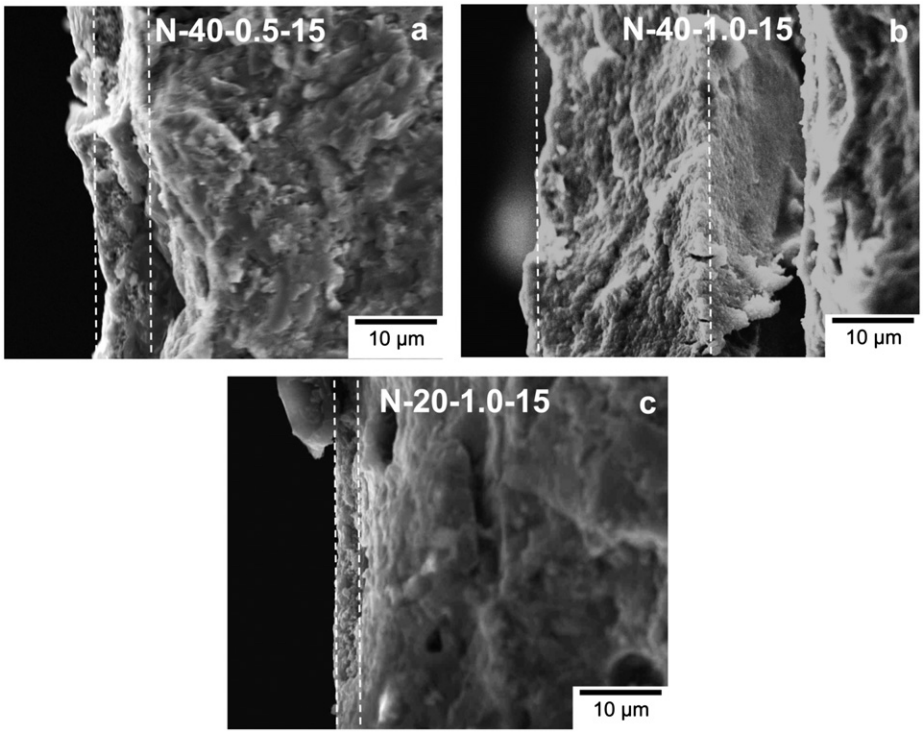

Fig. 7. Cross-sectional fracture surface microstructures (SEM) for: N-40-0.5-15 (a), N-40-1.0-15 (b), and N-20-1.0-15 (c).

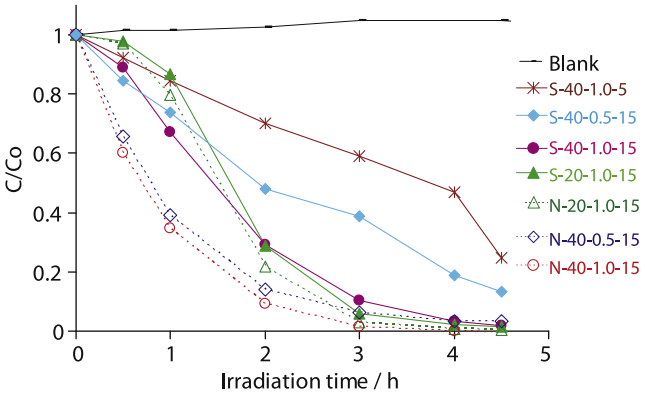

Fig. 8. Photocatalytic degradation of Methyl Orange solutions over the coatings. The result for the blank is also shown.

main phase. This is the case of TiO_2 thin films (anatase) obtained by spray pyrolisis deposition at 500 °C [35] which showed an efficiency in MO photodegradation of ~5% after 6 h of irradiation. When nanoporous anatase–TiO_2 films prepared by tape casting were used by the same authors [36], the MO degradation increased up to 30–60% after 6 h of irradiation. In both cases, the catalytic tests were carried out at pH 4.0 under three F18 W/T8 tubes (Philips) with a λ_{max} (emission) at 365 nm. Similar results were obtained by other authors [37] with nanoporous anatase-TiO_2 thin films prepared by spin-coating on glass substrates from a sol–gel solution with a MO degradation conversion of ~50% after 7 h irradiation. A photocatalytic degradation of ~55% was described [10] for stocked porous rutile-TiO_2 sheets sintered at 1000 °C after 5 h of irradiation. In that work, authors only used nanopowders and a Hg lamp (500 W). In this study we use a less power lamp (125 W), and a MO degradation conversion of ~91% was obtained just after 2 h of irradiation.

4. Conclusions

TiO_2 coatings have been produced from aqueous suspensions through a thermal gelation mechanism using agar as a gelling binder. The presence of gelling additive improves wetting on the commercial tile. This allows making use of the surplus tiles to obtain 'smart' tiles with corresponding economical and environmental advantages.

The thickness of the final coating increases with the concentration of polysaccharide, withdrawal rate and suspension solid loading. The attainable thickness is limited by the adherence between film and substrate. A wide range of thicknesses have been obtained by this procedure, from around 3 μm to near 30 μm.

The coating efficiency for MO degradation in presence of UV radiation increases by decreasing the grain size, and by increasing the withdrawal rate, agar content and solid loading of the precursor suspension. The most efficient coating for MO degradation was the nanostructured coating prepared from a 40 wt% nanosuspension with 1.0 wt% agar and obtained under a withdrawal rate of 15 mm s^{-1} (N-40-1.0-15). The degradation of a MO solution in presence

Table 1
Photocatalytic activity of selected sintered coated tiles.

Sample	Solid loading (wt%)	Agar content (wt%)	Withdrawal mm s^{-1}	K (h^{-1})/R^2	Degradation (%) t=2.0/3.0 h
S-40-1.0-5	40	1.0	5	0.1789/0.996	30/41
S-40-1.0-15			15	0.7308/0.976	71/90
S-40-0.5-15		0.5		0.4237/0.988	52/61
S-20-1.0-15	20	1.0		0.8168/0.968	71/94
N-40-1.0-15	40	1.0	15	1.2973/0.983	91/98
N-40-0.5-15		0.5		0.8918/0.991	86/94
N-20-1.0-15	20	1.0		0.9197/0.973	78/97

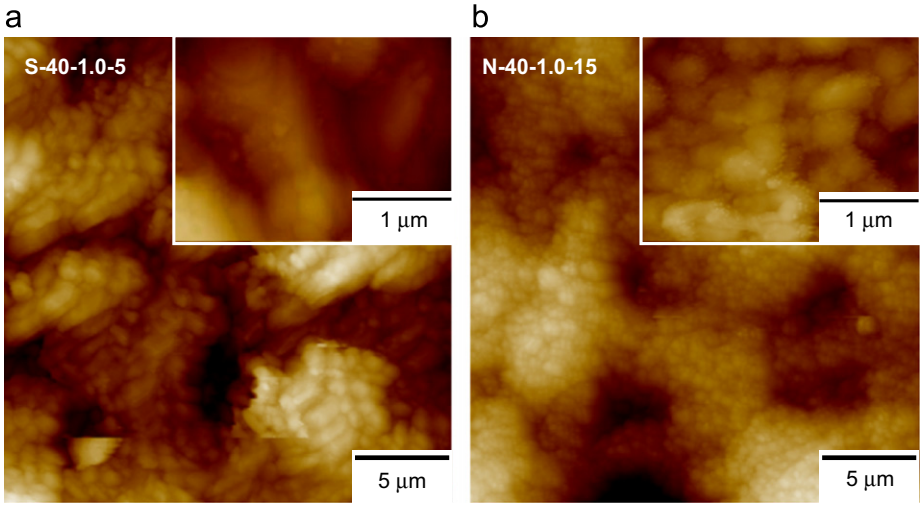

Fig. 9. Topographic images of a 25 μm × 25 μm section of the coatings: S-40-1.0-5 (a) and N-40-1.0-15 (b) showed by tapping mode AFM in air. The insets show a small section (5 μm × 5 μm) of the corresponding coatings.

of this coating was 91, 98 and 100% after 2, 3 and 4 h of irradiation.

Acknowledgements

This work has been supported by Spanish Ministry of Science and Innovation through MAT2010-15175 research grant, which is co-funded by FEDER. I.S. thanks a Ramón y Cajal fellowship (RYC-2008–03523). A. Natoli is thanked for experimental help in optimising the sub-micron suspension.

References

[1] A. Fujishima, X. Zhang, Titanium dioxide photocatalysis: present situation and future approaches, Comptes Rendus Chimie 9 (2006) 750–760.
[2] A. Folli, U.H. Jakobsen, G.L. Guerrini, D.E. Macphee, Rhodamine B discolouration on TiO_2 in the cement environment: a look at fundamental aspects of the self-cleaning effecting concretes, Journal of Advanced Oxidation Technologies 12 (2009) 126–133.
[3] R.S. Singh, V.K. Rangari, S. Sanagapalli, V. Jayaraman, S. Mahendra, V.P. Singh, Nano-structured CdTe CdS and TiO_2 for thin film solar cell applications, Solar Energy Materials and Solar Cells 82 (2004) 315–330.
[4] M. Mayo, Processing of nanocrystalline ceramics from ultrafine particles, International Materials Reviews 41 (1996) 1743–2804.
[5] M.N. Rittner, T. Abraham, Economics: nanostructured materials: an overview and commercial analysis, Journal of the Minerals Metals and Materials Society 50 (1998) 1160–1196.
[6] S.S. Madaeni, N. Ghaemi, Characterization of self-cleaning RO membranes coated with TiO_2 particles under UV irradiation, Journal of Membrane Science 303 (2007) 221–233.
[7] M. Hemissi, H. Amardjia-Adnani, J.C. Plenet, Titanium oxide thin layers deposed by dip-coating method: their optical and structural properties, Current Applied Physics 9 (2009) 717–721.
[8] A. Folli, C. Pade, T.B. Hansen, T. De Marco, D.E. Macphee, TiO_2 photocatalysis in cementitious systems: insights into self-cleaning and depollution chemistry, Cement and Concrete Research, http://dx.doi.org/10.1016/j.cemconres.2011.12.001.
[9] K. Dai, H. Chen, T. Peng, D. Ke, H. Yi, Photocatalytic degradation of methyl orange in aqueous suspension of mesoporous titania nanoparticles, Chemosphere 69 (2007) 1361–1367.
[10] L. Ren, Y.P. Zeng, D. Jiang, Preparation of porous TiO_2 sheets by aqueous tape casting and their photocatalytic activation, International Journal of Applied Ceramic Technology 5 (2008) 505–512.
[11] Y. Zhao, X. Hang, J. Zhai, J. He, L. Jiang, Z. Liu, S. Nishimoto, T. Murakami, A. Fujishima, Z. Zhu, Enhanced photocatalytic activity of hierarchically micro-/nano-porous TiO_2 films, Applied Catalysis B-Environmental 83 (2008) 24–29.
[12] Y. Ding, C. Yang, L. Zhu, J. Zhang, Photoelectrochemical activity of liquid phase deposited TiO_2 film for degradation of benzotriazole, Journal of Hazardous Materials 175 (2010) 96–103.
[13] R. Zhang, T. Oyama, S. Horikoshi, J. Zhao, N. Serpone, H. Hidaka, Photocatalytic decoposition of the sodium dodecylbenzene sulfonate surfactant in aqueous titania suspensions exposed to highly concentrated

solar radiation and effects of additives, Applied Catalysis B-Environmental 42 (2003) 13–24.
[14] K. Fan, M. Liu, T. Peng, L. Ma, K. Dai, Effects of paste components on the properties of screen-printed porous TiO_2 film for dye-sensitized solar cells, Renewable Energy 35 (2010) 555–561.
[15] X. Su, J. Zhao, Y. Li, Y. Zhu, X. Ma, F. Sunb, Z. Wang, Solution synthesis of Cu_2O/TiO_2 core–shell nanocomposites, Colloids and Surfaces A 349 (2009) 151–155.
[16] T. Aarthi, P. Narahari, G. Madras, Photocatalytic degradation of Azure and Sudan dyes using nano TiO_2, Journal of Hazardous Materials 149 (2007) 725–734.
[17] M. Vicent, E. Sánchez, I. Santacruz, R. Moreno, Dispersion of TiO_2 nanopowders to obtain homogeneous nanostructured granules by spray-drying, Journal of the European Ceramic Society 31 (2011) 1413–1419.
[18] K.K. Schuegraf, in: Handbook of Thin-Film Deposition Processes and Techniques, Noyes Publications, New York, 1995.
[19] R. Moreno, The role of slip additives in tape-casting technology: part I–solvents and dispersants, American Ceramic Society Bulletin 71 (1992) 1521–1530.
[20] H. Amorín, I. Santacruz, J. Holc, M.P. Thi, M. Kosec, R. Moreno, M. Algueró, Tape casting performance of ethanol slurries for processing textured PMN-PT Ceramics from nanocrystalline powder, Journal of the American Ceramic Society 92 (2009) 996–1001.
[21] I. Santacruz, K. Annapoorani, J. Binner, Preparation of high solids content nanozirconia suspensions, Journal of the American Ceramic Society 91 (2008) 398–405.
[22] I. Santacruz, M.I. Nieto, J. Binner, R. Moreno, Wet forming of concentrated nano $BaTiO_3$ suspensions, Journal of the European Ceramic Society 29 (2009) 881–886.
[23] L.P. Meier, L. Urech, L.J. Gauckler, Tape casting of nanocrystalline ceria gadolinia powder, Journal of the European Ceramic Society 24 (2004) 3753–3758.
[24] I. Santacruz, C. Baudín, M.I. Nieto, R. Moreno, Improved green properties of gelcast alumina through multiple synergistic interactions of polysaccharides, Journal of the European Ceramic Society 23 (2003) 1785–1793.
[25] I. Santacruz, M.I. Nieto, R. Moreno, Alumina bodies with near-to-theoretical density by aqueous gelcasting using concentrated agarose solutions, Ceramics International 31 (2005) 439–445.
[26] R. Moreno, B. Ferrari, I. Santacruz, M.I. Nieto, Spanish Patent, Publication No. ES 2 235 618, Concession Date 16/10/2006.
[27] ASTM 21-1272.
[28] ASTM 21-1276.
[29] I. Santacruz, M.I. Nieto, R. Moreno, P. Ferrandino, A. Salomoni, I. Stamenkovic, Aqueous injection moulding of porcelains, Journal of the European Ceramic Society 23 (2003) 2053–2060.
[30] S. Bueno, R. Moreno, C. Baudín, Reaction sintered Al_2O_3/Al_2TiO_5 microcrack-free composites obtained by colloidal filtration, Journal of the European Ceramic Society 24 (2004) 2785–2791.
[31] A. Natoli, A. Cabeza, A.G. De la Torre, M.A.G. Aranda, I. Santacruz, Colloidal processing and characterization of porous TiO_2 samples, Journal of the American Ceramic Society 95 (2012) 502–508.
[32] A.J. Millán, R. Moreno, M.I. Nieto, Thermogelling polysaccharides for aqueous gelcasting—part II: influence of gelling additives on rheological properties and gelcasting of alumina, Journal of the European Ceramic Society 22 (2002) 2217–2222.
[33] M. Ren, R. Ravikrishna, K.T. Valsaraj, Photocatalytic degradation of gaseous organic species on photonic band-gap titania, Environmental Science and Technology 40 (2006) 7029–7033.
[34] D. Beydoun, R. Amal, G. Low, S. Mcevoy, Role of nanoparticles in photocatalysis, Journal of Nanoparticle Research 1 (1999) 439–458.
[35] L. Andronic, A. Duta, TiO_2 thin films for dyes photodegradation, Thin Solid Films 515 (2007) 6294–6297.
[36] L. Andronic, D. Andrasi, A. Enesca, M. Visa, A. Duta, The influence of titanium dioxide phase composition on dyes photocatalysis, Journal of Sol–Gel Science and Technology 58 (2011) 201–208.
[37] B. Guo, Z. Liu, L. Hong, H. Jiang, Sol gel derived photocatalytic porous TiO_2 thin films, Surface and Coatings Technology 198 (2005) 24–29.